




## Research Article

# Experimental Investigations on Erosion-Corrosion Characteristics of HVOF-Sprayed WC-10% Ni Coatings Deposited on Aluminum Alloy

G. S. Pradeep Kumar,<sup>1</sup> Sampreeth Sunkad,<sup>2</sup> R. Jogeshwar,<sup>2</sup> R. Keshavamurthy ,<sup>3</sup> Vijay Tambrallimath ,<sup>4</sup> Sasidhar Jangam,<sup>1</sup> and Dadapeer Basheer <sup>5</sup>

<sup>1</sup>Department of Mechanical and Automobile Engineering, Christ University, Bangalore 560074, Karnataka, India

<sup>2</sup>Automobile Engineering, Christ University, Bangalore 560074, Karnataka, India

<sup>3</sup>Department of Mechanical Engineering, Dayananda Sagara College of Engineering, Bangalore-560078, Karnataka, India

<sup>4</sup>Department of Aeronautical and Automobile Engineering, Manipal Institute of Technology, Manipal Academy of Higher Education, Manipal 576104, Karnataka, India

<sup>5</sup>Department of Mechanical Engineering, Haramaya Institute of Technology, Haramaya Univeristy, Dire Dawa 138, Ethiopia

Correspondence should be addressed to Vijay Tambrallimath; [drvijaytmath@gmail.com](mailto:drvijaytmath@gmail.com) and Dadapeer Basheer; [dadapeer.basheer@haramaya.edu.et](mailto:dadapeer.basheer@haramaya.edu.et)

Received 24 June 2022; Revised 22 July 2022; Accepted 5 August 2022; Published 13 February 2023

Academic Editor: Waleed Fekry Faris

Copyright © 2023 G. S. Pradeep Kumar et al. This is an open access article distributed under the Creative Commons Attribution License, which permits unrestricted use, distribution, and reproduction in any medium, provided the original work is properly cited.

The current work investigates the erosion-corrosion behaviour of thermally sprayed tungsten carbide-10% nickel (WC-10% Ni) coatings placed on the AA6061 aluminum alloy. The AA6061 aluminum alloy was coated with tungsten carbide –10% nickel coatings utilising a high-velocityoxy-fuel (HVOF) spray method. The microstructure and hardness of thermally sprayed coatings were examined using a scanning electron microscope (SEM) and a Vickers hardness tester. The slurry erosion-corrosion wear tests were carried out by varying the parameters of the slurry erosion process, such as testing time, slurry content, slurry speed, and impinging particle size, on the erosion testing equipment. The data demonstrated that when slurry concentration, slurry speed, and impinging particle size increased, so did the slurry erosion-corrosion wear loss. The wear processes of uncoated and thermally sprayed tungsten carbide –10% nickel have been examined using SEM and a 3-D confocal microscope.

## 1. Introduction

Longer service life, particularly in harsh environments, and lower density design considerations are critical factors in today's engineering industry. Many advanced high-performance machines are subjected to increasingly hostile conditions such as high temperatures and severe corrosive, frictional, tribological, and erosive attacks during normal operation. As a consequence of this, essential components are unable to survive the rigours of tough working circumstances, which in turn causes the economy of the industry to suffer. As a consequence of this, complex engineering components call for materials with a specific

mix of qualities that regular metals, alloys, polymers, and ceramics are unable to deliver for themselves. Materials that are used in the automotive, aerospace, marine, energy, and chemical industries, among others, ought to be able to satisfy such prerequisites. The fundamental objective is to improve the surface-related properties of matter so that high-quality components may be produced that account for all surface phenomena while maintaining a competitive position in the market. Commercial surface coating processes include electrodeposition, weld-overlay, cladding, chemical vapour depositions, physical vapour depositions, thermal spray coating, and electroplating. Surface modification techniques include flame beam hardening (FBM), induction beam

hardening (IBM), laser beam hardening (LBM), electron beam hardening (EBM), highly energetic, and diffusion treatments. Combining surface coating treatments and surface modification techniques can improve surface qualities, resulting in unique needs and functionality. Between these, the thermal spray approach appears to be a prominent, effective, and cost-effective surface modification technology. It performs admirably in terms of antioxidation/corrosion, antithermal degradation, and antiwear properties [1–6].

The technology of thermal spraying enables a variety of coating processes. This procedure involves pushing soft particles or partial and fine molten towards the surface of the component. Once there, they are exposed to a rapid influence that causes them to flatten and solidify. The high-velocityoxy-fuel (HVOF) technique is recommended as one of the best thermal spraying techniques for coatings deposition due to its unique characteristics, such as low temperature and high-velocity particle deposition. In addition, the high-velocityoxy-fuel (HVOF) technique is one of the most recently developed thermal spraying methods. During the spraying process, this technology degrades the feedstock less than other spray coating processes. This particular deposition technique can produce coatings of superior quality due to the aforementioned positive characteristics, such as oxide concentration, densities, less porosity, wear resistance, and higher hardness. The choice of coating materials or feedstocks for high-velocityoxy-fuel spray coatings is crucial and requires extensive evaluation of the substrate and applications. High-velocity oxy fuel-sprayed materials such as chromium, silicon carbide, carbon monoxide, titanium dioxide, tungsten carbide, and aluminum oxide are used to improve wear and corrosion behaviour in industries such as printing and mining machinery, aircraft, automobile, shipping, and textiles. In contrast, wrought iron carbide is widely acknowledged as a hard ceramic material with superior mechanical, physical, and chemical properties that outperform all other ceramic materials [7–11].

Because of their higher melting temperatures, hardness, and chemical resistance, tungsten-based compounds have been found to be more significant in applications such as wear-resistant and corrosion-resistant [12–14]. Hermanek [15] used a high-velocityoxy-fuel spray method to coat turbine steels with chromium oxide coatings, and their performance was evaluated in slurry erosive environments. The effects of three factors on these materials' slurry erosion were investigated: slurry content, average particle dimension, and speed. When compared to uncoated steels, chromium oxide coating components sprayed with high-velocityoxy-fuel resulted in improved erosion-corrosion resistance. According to the author, high-velocityoxy-fuel spray chromium oxide coatings improve slurry erosion-corrosion resistance because they increase hardness.

Vuoristo [16] compared six thermal spray coatings to untreated martensite corrosion-resistant steel in terms of cavitation and slurry erosion-corrosion behaviour. The oxy-fuel technique was used to coat the Ni, W, and Cr, and the high-velocityoxy-fuel technology was used to create the WC surface coatings. The coatings' cavitation erosion-corrosion

behaviour resistance was evaluated using vibratory instrumentation, and slurry corrosion studies were carried out in a modified centrifugal pump in accordance with ASTM G32 standards. Talib et al. [17] compared martensite corrosion-resistant under unprotected conditions to 70%Ni-30%Cr coatings deposited by the high-velocityoxy-fuel spray process in terms of cavitation erosion-corrosion and slurry erosion behaviour to 70%Ni-30%Cr coatings deposited by the high-velocityoxy-fuel spray process. The resistance of thermal sprayed surfaces to the synergistic influence of slurry and cavitation erosion-corrosion was investigated using a slurry pot tester with prismatic bluff bodies as cavitation inducers.

A high-velocityoxy-fuel spray coating has improved the erosion-corrosion resistance of S410 slurry. When unprotected samples are compared to high-velocityoxy-fuelspray-coated samples, it is discovered that the unprotected samples have weak erosion-corrosion resistance, implying that when placed through the erosion tester under the same test conditions, the high-velocityoxy-fuelspray-coated samples have greater erosion-corrosion resistance.

Aluminum alloys are among the most important, efficient, and well-known industrial materials. This alloy in particular has excellent electrical and thermal conductivity, a higher specific strength, is less expensive than many other alloys, and is relatively easy to shape. Aluminum alloys of the 6xxx series, alloyed with Si and Mg, are now much more desirable in technical applications such as naval fields, automotive, and aerospace applications due to their improved fatigue life, improved manufacturability, and higher strength to weight ratio. However, when compared to other structural parts, 6xxx series aluminum has poor surface properties, such as lower wear resistance and hardness [18, 19]. As a result of the importance of surface properties, many technical applications are limited. Keshavamurthy et al. [20] investigated the wear properties of CrO<sub>2</sub>-TiO<sub>2</sub> composite coatings produced on AA6061 using the high-velocityoxy-fuel process. Tribological, microstructural, and hardness tests were all performed on the synthetic coatings. They discovered that when compared to AA6061, the composite coatings have a hardness that is more than 50%. When compared to unprotected aluminum alloy, coated aluminum alloy has a wear rate that is 50% lower and a coefficient of friction that is 13% lower than the unprotected aluminum alloy. Both the substrate and the coatings will experience an increase in their rate of wear and their coefficient of friction in proportion to the load and sliding velocity. There are very few investigations on high-velocityoxy-fuel sprayed tungsten-based coatings with 10% nickel applied to AA6061 alloys, as indicated by the research that was evaluated in the relevant literature. In addition, there are no data available on the slurry erosion-corrosion behaviour of high-velocityoxy-fuel sprayed tungsten-based coatings with 10% nickel applied to AA6061 alloy under a variety of slurry test conditions. There are a number of elements that should be taken into consideration, including the particle impeding size, rotational speed, sand content, and test durations. As a consequence of this, the purpose of this research is to investigate the slurry erosion-corrosion behaviour of

high-velocity oxy-fuel-sprayed chromium oxide coatings on aluminum 6061 alloy substrates by utilising a slurry erosion-corrosion test setup and to investigate the erosive wear mechanisms that are involved by utilising a scanning electron microscope and a confocal microscope.

## 2. Materials and Methods

AA6061 aluminum alloy was preferred as a substrate component because these are widely employed in automobiles, aircraft, and shipbuilding industries. AA6061 aluminum alloy shows high strength to weight ratio and high corrosion and wear rate. Table 1 shows the elemental composition of AA6061 aluminum alloy. Commercially used coating powder of tungsten carbide with 10% nickel (WC-10% Ni) was used as a feedstock agent. The morphology of WC-10% Ni feedstock powder was captured by the scanning electron microscope as shown in Figure 1 along with EDS maps. The powdered tungsten carbide with 10% nickel was identified to show a round and elliptical shape.

By utilising a sophisticated high-velocity oxy-flame thermally coated setup, coating studies were carried out at M/s Spraymet Technology Pvt. Ltd., Bangalore, Karnataka, India. 25  $\mu\text{m}$  of Ni-Mo-Cr adhesion coating was placed prior to WC-10% Ni deposition, and two kinds of samples with 100 m and 200 m coating thickness were generated on the AA6061 aluminum substrate. Prior to the cleaning and surface creation, the adhesion coating was applied to the AA6061 aluminum substrate. Using a single-torch high-velocity oxy-flame gun and typical deposition circumstances, a Ni-Mo-Cr adhesion coating of 25  $\mu\text{m}$  with nominal particle size distribution was high-velocity oxy-flame-deposited on the substrate. Table 2 shows the high-velocity oxy-flame processing conditions that were used to deposit the topcoat. Prior to high-velocity oxy-flame coatings, the AA6061 aluminum substrate was sandblasted with alumina ( $\text{Al}_2\text{O}_3$ ) to increase the surface roughness and clean the surface to ensure good adherence to WC-10% Ni coating.

The microstructural investigations, hardness analysis, and slurry erosion-corrosion studies have all been performed on the WC-10% Ni coating that has been produced. Optical microscope (OM) and scanning electron microscope were employed to capture the cross sections and upper surface of the coatings.

Before capturing under a microscope, the coated samples were sliced with a wire-cut electrical discharge machine to the required dimensions, polished well with various grits of emery papers followed by disc polishing using velvet cloth, and the samples were then etched in the suitable etchant for sufficient time to reveal the microstructural features. The Vickers hardness test was performed according to ASTM E-92 criteria. Hardness was measured on a cross section with a load of 0.1 kg and a dwell time of 15 seconds. Hardness values were collected on each sample, and the average value of all six indentations was taken into account. The erosion-corrosion behaviour of the high-velocity oxy-flame-sprayed WC-10% Ni coatings was assessed using a pot-kind slurry erosion tribometer. Prior to the slurry erosion-corrosion

investigations, samples were measured with a 0.01 mg accuracy electronic balance, specimens were washed in an ultrasonic bath with acetone as ultrasonic media and dried with warm removing the moisture content, and a similar procedure was followed well after the erosion-corrosion investigation to eliminate unnecessary debris on the sample surface. Figure 2 shows the dimensions of the slurry erosion test specimen. Silica sand has been used as an erodent in all experiments. The slurry mixture was made with a certain proportion of silica sand and water. Erosion-corrosion tests were carried out on both uncoated and WC-10% Ni-coated AA6061 alloys under varied test circumstances [11–13]. During the erosion-corrosion examination, the slurry content varied from 50 g/l–200 g/l, the testing duration was adjusted from 5 hours–20 hours, and erodent particle sizes of 210 m, 312 m, 400 m, and 625 m were utilised. At 500 rpm increments, a peak slurry speed of 1500 rpm was used. After the slurry erosion-corrosion examination, samples were analyzed under SEM and a confocal microscope to determine possible material removal mechanisms and the level of destruction in both uncoating and coating specimens. Figure 3 shows the slurry erosion wear tester.

## 3. Results and Discussion

*3.1. Microstructure.* The optical microstructures of high-velocity oxy-fuel-sprayed WC-10% Ni coatings deposited on an AA6061 aluminum substrate are depicted in Figures 4(a) and 4(b). The microstructures reveal that the coatings are composed of a relatively homogeneous, lamellar deposit. In the presence of WC-Ni bind coating, coatings exhibit seamless binding with the AA6061 alloy substrate, as evidenced by SEM of cross sections. In addition, two top and cross-sectional images reveal a thick coating deposition with few flaws. It is also evident that the lamella-like structure contains minimal discontinuities, such as small pores. Figures 4(c) and 4(d) depict the SEM microstructures of cross-sectional and surface-developed coatings. SEM microstructures at high resolution reveal the existence of lamella-like structures throughout the thickness. In certain areas, micro holes were discovered both within and between the splats. The impact of completely or partially molten WC-10% Ni particles in applied coatings can cause small pores and fractures; WC-10% can undergo severe deformation. Ni particles cause splat fracturing. The entrapment of non-melted particles is most likely caused by rapid solidification. The porosity concentration of manufactured coatings is heavily influenced by tungsten carbide-10% nickel powder.

The porous dispersion is influenced by the shape, dimension, dispersion, and thermal properties of WC 10% Ni. Furthermore, spray factors such as particle speed, spray angle or spray distance, temperatures, and holding time play an important effect in porous morphology and volumes. Scanning electron microscope analysis of cross-sectional areas of formed coatings reveals the most frequent morphological characteristics of high-velocity oxy-fuel coatings. Rarely observable microscopic pores were scattered all through morphology based on meticulous examinations of cross-sectional pictures demonstrating the existence of both

TABLE 1: Composition of aluminum alloy.

Element	Composition (wt. %)									
	Mg	Si	Fe	Cu	Mn	Pb	Zn	Ti	Others	Al
AA6061 alloy	0.75	0.9	0.8	0.38	0.29	0.03	0.009	0.02	—	Balance

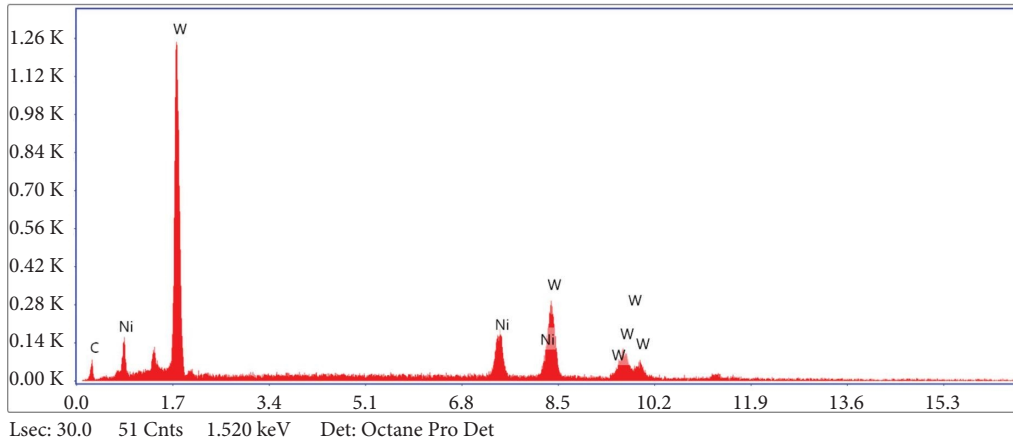
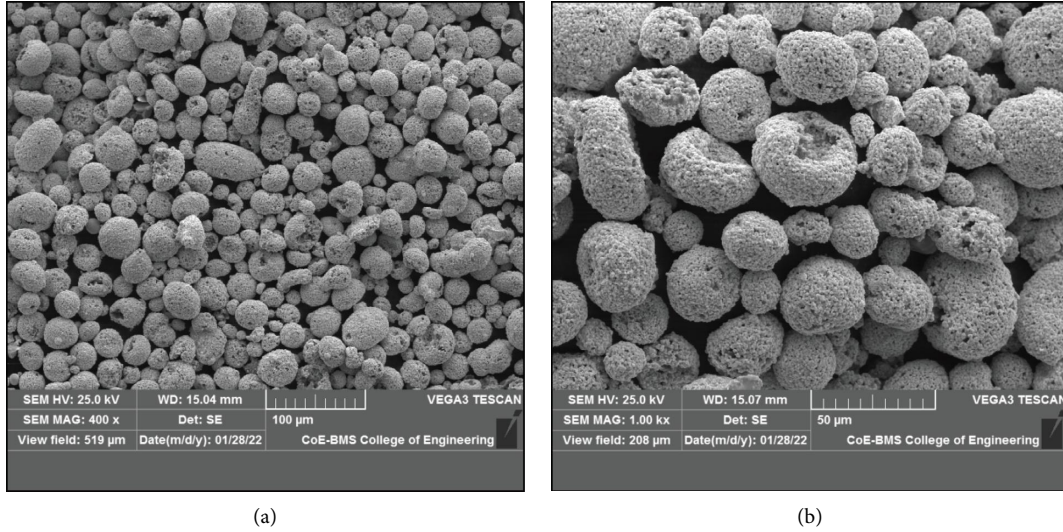


FIGURE 1: SEM and EDS of WC + 10% Ni feed stock powder.

TABLE 2: HVOF process conditions.

SI NO	Parameter	Value
1	Liquid petroleum gas	$2 \times 10^{-3} \text{ m}^3/\text{s}$
2	Oxygen flow rate	$4.5 \times 10^{-3} \text{ m}^3/\text{s}$
3	Air flow	$5 \times 10^{-3} \text{ m}^3/\text{s}$
4	Nitrogen carrier gas	$2.8 \times 10^{-3} \text{ m}^3/\text{s}$
5	Feed stock rate	$0.6 \times 10^{-3} \text{ kg/s}$
6	Standoff distance	1.8 metres
7	Feed stock size	30–45 microns

nonmelted and semimelted WC-10% Ni powdered particles and lamella kind of structures. As demonstrated in the preceding section, they can be found at the intersection of lamella splats inside the coating matrix, as well as in some nonmelted or semimelted WC-10% Ni particles.

Altogether, the developed coatings stuck well under optimal conditions, with thick and uniform deposition in both cases [20, 21].

**3.2. Hardness.** At an indent load of 0.1 kg and a dwelling time of 15 seconds, the hardness changes in AA6061 substrate and WC-10% Ni coatings are illustrated in Figure 5. When compared to an untreated AA6061 substrate, WC-10% Ni coatings showed a 10-fold increase in microhardness. Unprotected AA6061 substrate had a mean microhardness of 75 VHN, whereas 100um WC-10% Ni coatings had a mean microhardness of 610 VHN, this simply proves that the microhardness of coatings rises as the thickness of the coating increases. As tungsten carbide is a harder ceramic, it generally requires a high microhardness value. This



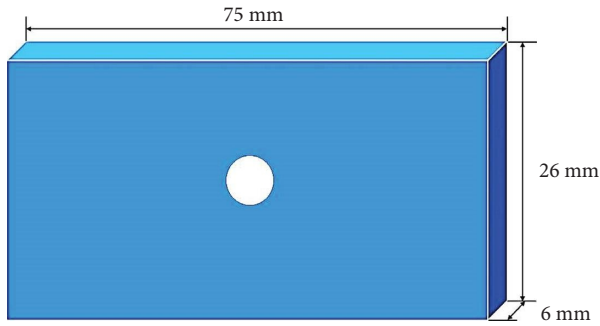


FIGURE 2: Dimensions of slurry erosion test specimens.

large increase in microhardness can be attributed to the fact that tungsten carbide is a harder ceramic with excellent microhardness even at higher temperatures, making it ideal for wear-resistant purposes. The inclusion of stable-tungsten carbide with a structure is known to increase the coatings' microhardness and ductility. Less permeability, thick depositing, and a homogeneous morphology all contribute to WC-10% Ni coatings' greater microhardness. The crystalline phase of oxide phases can be used to predict the properties of WC 10% Ni coatings. A very well oxide phase should have improved mechanical characteristics. The reality that the particulates plunge deeply into the substrate surface during the early coating attempts of deposits with a  $100\ \mu\text{m}$  thickness may account for the increased microhardness with an increment in coating thickness. The substrate can form better adhesions, but they will not stretch far enough to keep tiny pores and imperfections hidden. The very first layers of WC-10% Ni sprayed on AA6061 alloy substrates are likely to develop small pores and fracture.

As the coating thickness increases, the permeability begins to diminish. This could be because when multiple layers are formed on the same substrates, the fresh WC-10% has a higher velocity impact. In future trials, Ni powdered particles peen the previously deposited layers, resulting in effective densification. Kumar et al. [22] found that as coating thickness increases, the developed layers become thicker and less susceptible to peening, and that thicker coatings always have lower porosity and microhardness than thinner coatings.

### 3.3. Erosion-Corrosion Properties

**3.3.1. Effects of Coating.** Figure 6 shows the pictorial depiction of impact of high-velocity oxy-fuel-sprayed WC-10% Ni coatings on the erosion-corrosion performance of AA6061 alloy substrate. Figure 6 depicts that the coatings offer excellent wear resistance by demonstrating the lower weight loss under identical test conditions. Superior surface hardness, corrosion resistance, and good adhesion between substrate and coatings are the primary reasons for enhanced erosion-corrosion performance of the coatings compared to uncoated alloy. Tungsten carbide (WC) and nickel influence the hardness and erosion-corrosion behaviour of coated AA6061 aluminum alloy. It is well known that the WC is a harder ceramic material. During the hardness test, the WC

coating applied on the AA6061 has the ability to withstand the indent load and resulted in small size indentation on the sample surface. Further, during the slurry erosion test, the WC coating does not allow the abrasive particles to penetrate into the AA6061 alloy substrate. It was also identified from the results that the erosion-corrosion resistance of the AA6061 aluminum alloy intensified after coating with tungsten carbide. Moreover, the enhancement in hardness due to tungsten carbide coating is a strong motive for high wear resistance. This phenomenon is achieved due to the protection of an alloy substrate with tungsten carbide coating, which contributed to the AA6061 alloy matrix strengthening by solid solution. Generally, tungsten carbide ceramics are because of the presence of covalent bond and ionic bond together and a greater amount of energy is required to fracture them as a consequence of the existence of the ionic bond. High hardness can be attained for the AA6061 alloy after coating with sufficient quantity of ceramic particles, which resulted in enhanced erosion-corrosion wear resistance. Because of the abovementioned reasons, the hardness and erosion-corrosion resistance of AA6061 alloy is greatly enhanced after coating. In addition to the WC, the 10% Ni coating also plays a crucial role in deciding the hardness and erosion-corrosion behaviour of coated AA6061 alloy. Generally, the coating of Ni on the AA6061 alloy provides a solid solution strengthening and leading to enhanced hardness as compared to the coated alloy. It also controls the possibility of galvanic coupling between the aluminum matrix and other constituents and retards electrochemical activity in the coated alloy and results in a less corrosion rate than the uncoated AA6061 alloy [23–25]. Finally, the protective coating consists of tungsten carbide with the optimized content (i.e. 10%) of nickel acquired combined properties of both elements such as solid solution strengthening, high hardness and wear resistance, and retardation of electrochemical activity, resulting in better properties of coated AA6061 alloy than the uncoated one.

**3.3.2. Influence of Slurry Concentration.** Figure 7 is a graphical representation of the effect of slurry content on the erosion-corrosion performance of an AA6061 alloy substrate and high-velocity oxy-fuel-sprayed WC-10% Ni coatings. Weight loss increases approximately linearly with increasing slurry concentration, as shown in Figure 7. For all studied concentrations, untreated AA6061 alloy and WC-10% Ni coatings exhibited an ascending trend. In addition, when compared to unprotected AA6061 alloy, WC-10% Ni coatings have a significantly reduced weight loss across all examined slurry content values. According to Kumar et al. [22], coatings lose 2 to 3 times less weight than uncoated AA6061 aluminum alloy for all slurry contents. Since weight loss increases gradually, there is a marginal decrease at extremely high slurry concentrations. The marginal decrease in weight loss with increasing slurry concentrations is most likely due to the shielding effect of ricocheted particles. After impacting the targeted surface, the ricocheted particles will interact with incoming new particulates, limiting the effect on the targeted surface or decreasing particle velocity.



FIGURE 3: Slurry erosion wear test: (a) slurry erosion wear tester, (b) slurry solution, and (c) mounted test specimen.

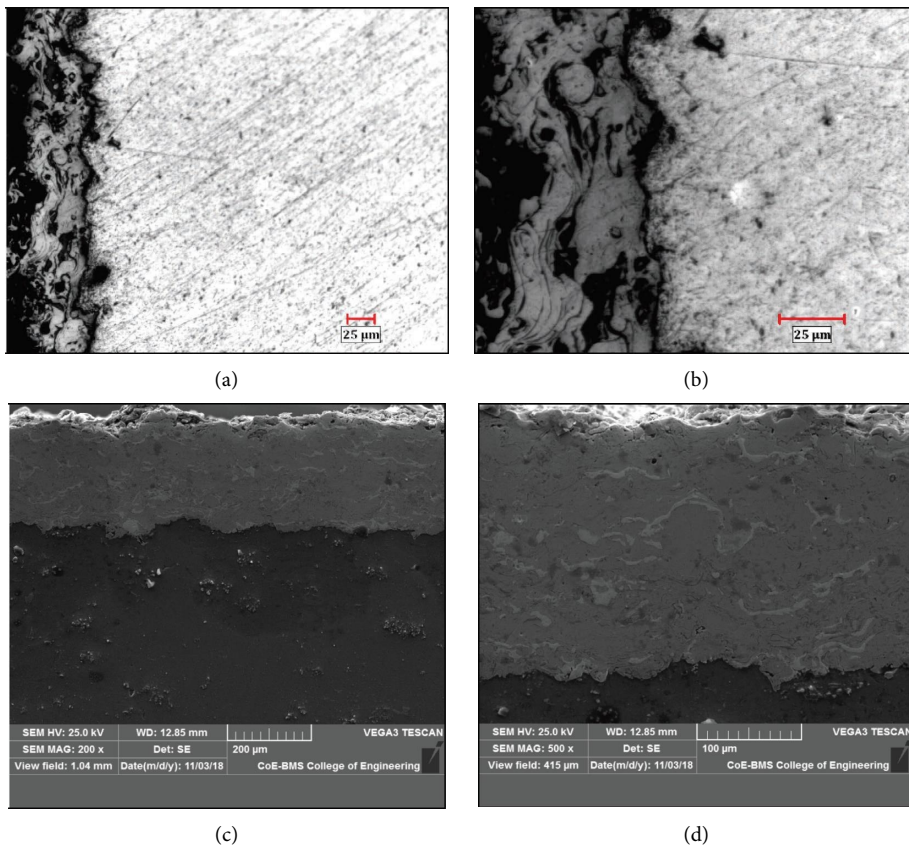


FIGURE 4: Optical and SEM images of WC-10% Ni coatings.

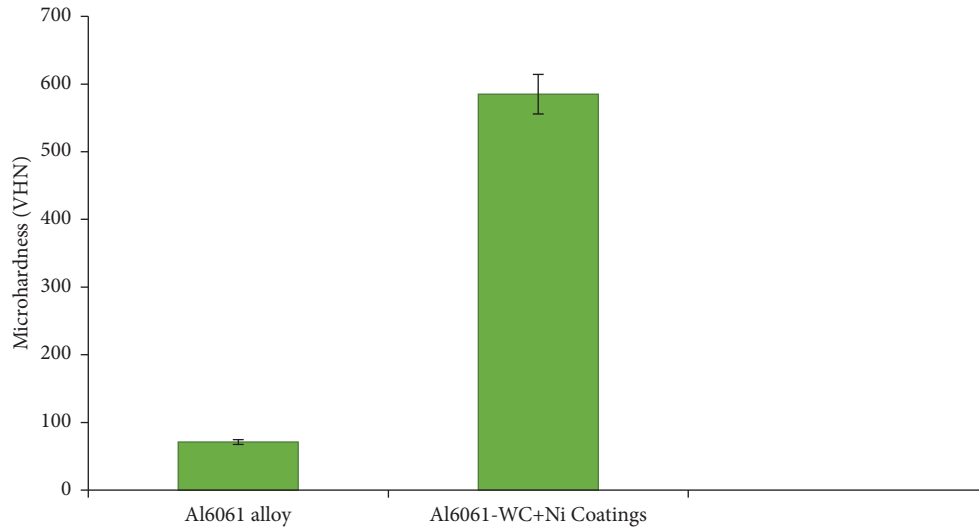


FIGURE 5: Comparison of hardness between alloy and coatings.

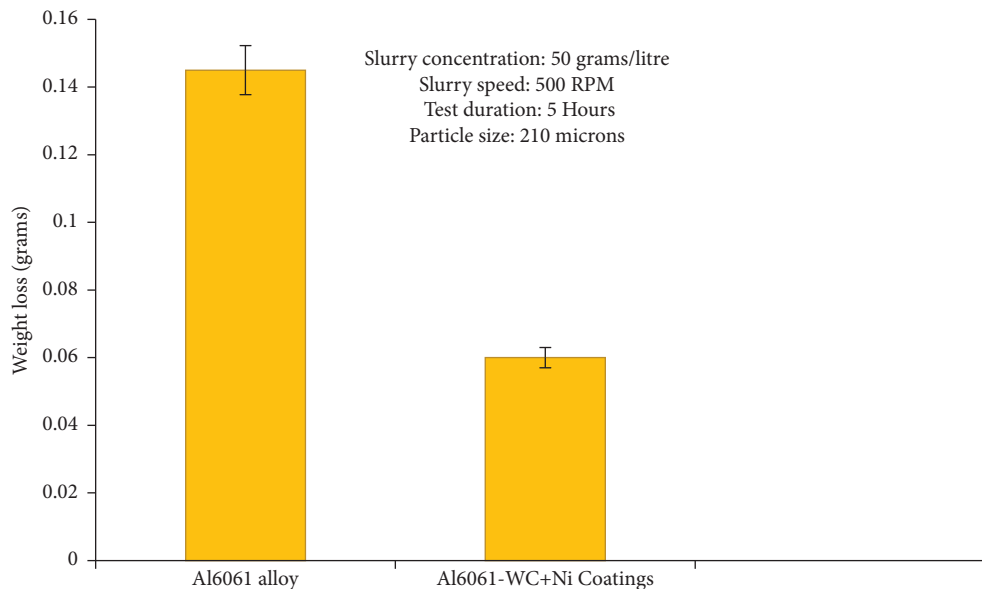


FIGURE 6: Comparison of slurry erosive wear between alloy and coatings.

However, the ricocheted particles will collide with newly arriving particles, altering their paths and causing them to strike the target at angles other than those initially specified. In addition, different impingements are possible based on the velocity and angle of collision of the impacting particles. Consequently, the reflected particles must collide once more [26]. The graph illustrates that the losing weight curve remains stable after 150 g/l and that the losing weight values for uncoated AA6061 and WC-10% Ni coatings are greater at high slurry concentrations than at low slurry concentrations. This could be explained by the fact that a greater number of particles would be available to strike the target surface at higher slurry concentrations than at lower concentrations, resulting in greater material loss.

Furthermore, because of the fluid's high viscosity, slurry particulates are pushed to follow the streamline and

change position close to the aimed surface, preventing the creation of a protective barrier. During the erosion-corrosion examination, slurry particles first begin to impact the surface, then shift directions closer to the aim and further away [27, 28]. WC-10% Ni coatings had shown significant weight reduction in comparison to unprotected AA6061 substrate at all slurry contents investigated. Furthermore, when the coating thickness grows, the weight loss rises.

**3.3.3. Influence of Slurry Speed.** Figure 8 shows the weight reduction variation of uncoated AA6061 alloy and high-velocity oxy-fuel-coated WC-10% Ni samples with varying slurry rotational speeds of 500 rpm, 1000 rpm, and 1500 rpm with constant exposure period, sand content, and particle size. In the context of unprotected AA6061 aluminum

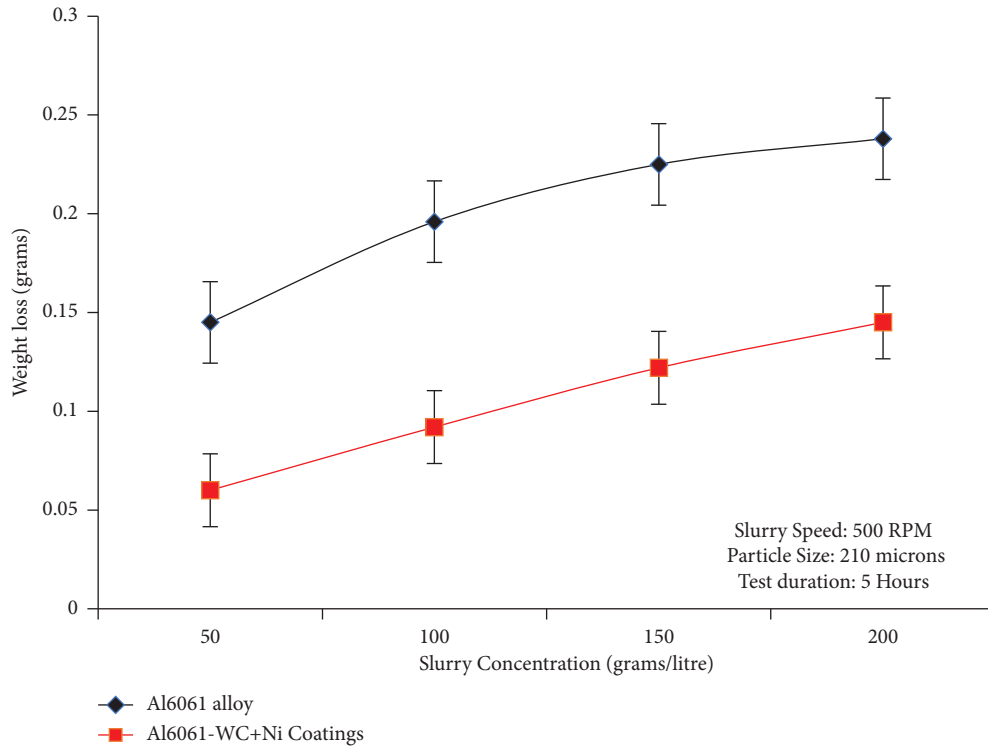


FIGURE 7: Influence of slurry concentration on slurry wear performance.

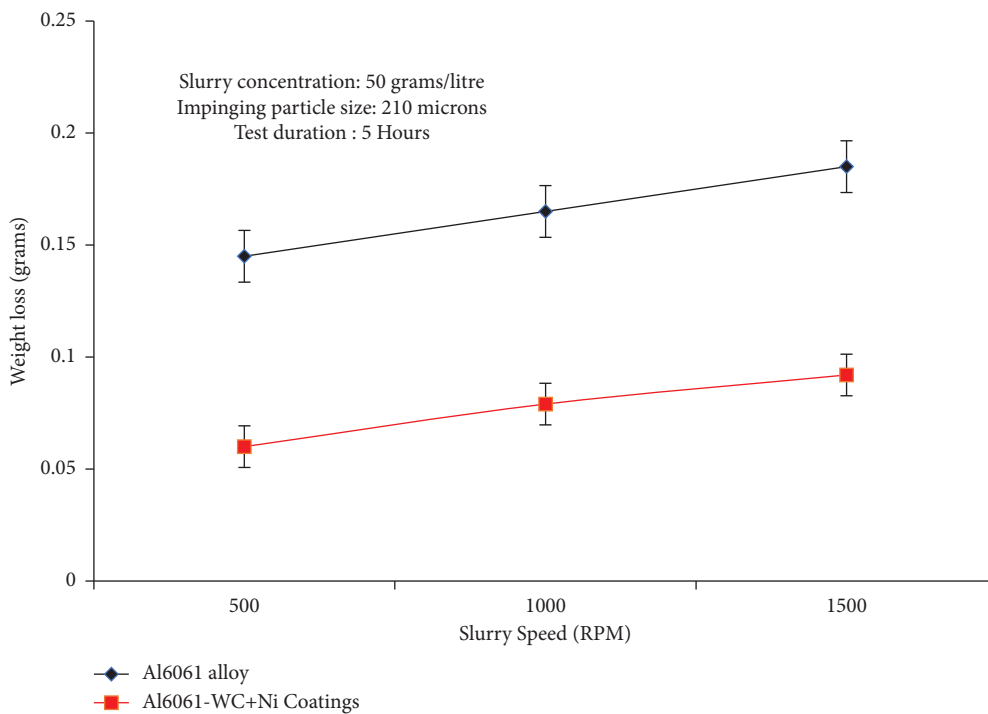


FIGURE 8: Influence of speed on slurry erosive wear.

substrate and WC-10% Ni-coated samples, higher weight reduction had increased continually when the slurry rotational speed increased. The testing duration, infringing particle size, and sand content were all kept constant at 5 hours, 210 metres, and 50 grammes, respectively, while the

slurry rotating speed was adjusted in increments of 500 rpm. It was discovered that when the slurry rotational speeds increased, the weight reduction of all specimens increased for both circumstances. Under slurry rotational speeds of 500 rpm, 1000 rpm, and 1500 rpm, unprotected AA6061

aluminum alloy lost a mean of 0.14 g, 0.16 g, and 0.18 g, respectively. High-velocity oxy-fuel coatings have been demonstrated to be more erosion-corrosion resistant than unprotected AA6061 aluminum alloy.

These findings suggest that the deposit of a WC-10% Ni coating improves the AA6061 alloy's erosion-corrosion resistance. The weight reduction for both unprotected AA6061 alloy and WC-10% Ni-coated samples continues to rise as the slurry rotational speed increases. The frequency of slurry concentration on the surface rises as the slurry rotational speed increases for a fixed content of slurry, resulting in greater weight reduction. The high slurry rotational speed enhances the kinetic energy and mass transfer of the particulates in the slurry, resulting in faster metal removal and more frequent particle impinge.

**3.3.4. Influence of Impinging Particles' Size.** The variation in the weight reduction of unprotected AA6061 alloy and WC-10% Ni aluminum coatings with varying infringing particle sizes is depicted graphically in Figure 9. In unprotected AA6061 alloy and WC-10% Ni coatings, the figure depicts a rise in infringing particle size, which has resulted in increased material removal. The coated AA6061 alloys, on the other hand, have been shown to lose significantly less weight than unprotected AA6061 alloys throughout all particle sizes. Furthermore, as the coating thickness increases, weight reduction reduces. The number of particles obtainable with tiny particles is more than the number of particles accessible with bigger particles at a particular slurry content.

Smaller sand particles contained less mass and impact energy, and they frequently deviated from the targeted surface immediately prior to the contact. Another two explanations for reduced weight reduction with tiny particles are intercolliding amongst the slurry particulates and deceleration after the strike; due to decreased kinetic energy, tiny slurry particulates do not show sufficient load to commence material erosion on the test sample surface. Considerable sand particles, on the other hand, have a higher impact strength and are capable of hitting the sample surface and removing metal off the targeted surface. Furthermore, due to its high mass and bigger contact region, big sand particles immediately become abrasive on the sample surface. When tiny particles impact the sample surface, a larger number of particles are present, yet when bigger particles for the same quantity impact the sample surface, every particle has high kinetic energy and destroys a greater area. Tiny particles have less inertia, resulting in less weight reduction. Tiny sand particles quickly become stuck in fluid streamline, resulting in randomized collisions with other particles and cylindrical walls; tiny particles contact the targets at a much slower speed than larger particles. The previous study by Lynn et al. [29] proved that as particle size drops, the colliding effectiveness of the sand grains reduces as well. Due to their greater inertia and colliding effectiveness, larger particles endure modest retardation before impacting on the targeted surface. Through all infringing particle sizes investigated, the weight reduction of coated AA6061 alloy with WC-10% Ni was much less than that of the unprotected AA6061 alloy in the current study. When the particle size is

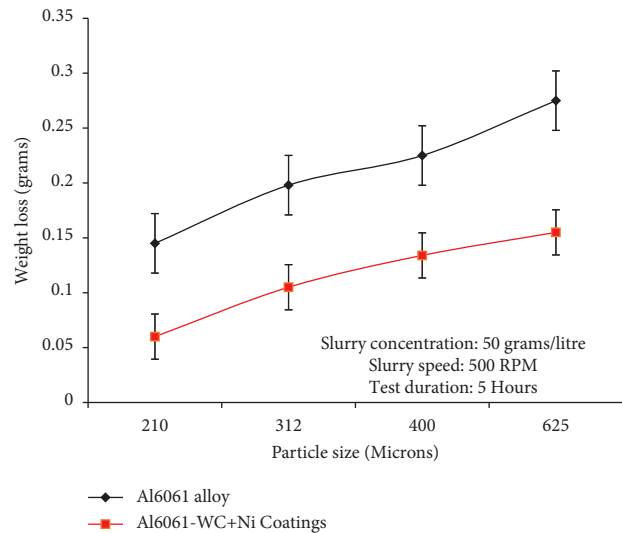


FIGURE 9: Influence of particle size on slurry erosive wear.

raised from 210 m to 625 m in an unprotected AA6061 alloy, the weight reduction increases by 62%.

**3.3.5. Influence of Test Duration.** Figure 10 depicts the results of an investigation into the weight reduction measured erosion-corrosion of high-velocity oxy-fuel-sprayed WC-10% Ni coatings and unprotected AA6061 aluminum alloy over various time periods. As the test length increases, the weight reduction of all specimens increases. In addition, it was noticed that as the test period is extended to fifteen hours, the weight loss of both uncoated and coated alloys increases; the weight loss appears to be steady. This may be due to the assurance that the desired surface will harden as a result of slurry particles' constant impending action. In addition, as the suspended slurry interacts with the particles, their crispness and hardness deteriorate over time. The duration of the test varied from 5 to 20 hours in 5-hour increments, while the slurry concentration, infringing particle size, and slurry rotational speed remained constant at 50 g/l, 210 m, and 500 rpm, respectively. It was found that as the duration of the experiment increased, weight loss increased in every specimen. It has also been realised that the WC-10% Ni coating on the AA6061 alloy reduces weight loss. The maximum weight loss for AA6061 alloy was 0.14 g after 5 hours, 0.20 g after 10 hours, 0.28 g after 15 hours, and 0.29 g after 20 hours of testing, respectively.

The WC-10% Ni-coated AA6061 aluminum alloy with 100  $\mu\text{m}$  lost 0.05 g, 0.09 g, 0.115 g, and 0.126 g throughout the course of 5 hours, 10 hours, 15 hours, and 20 hours of testing, respectively. The present findings clearly show that the deposit of WC-10% Ni coatings improves the hardness of AA6061, hence increasing its erosion-corrosion resistance. Furthermore, if the test length is prolonged from 5 hours to 15 hours, weight reduction for coated and uncoated alloys starts to rise. It has been discovered that increasing the time length leads to better mass loss for up to 15 hours, after which it becomes nearly steady. The constant behaviour after fifteen hours could be due to a variety of factors; for example,



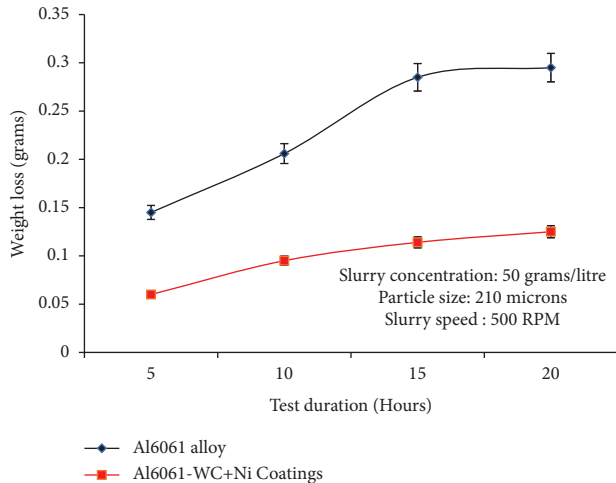


FIGURE 10: Influence of test duration on slurry erosive wear.

in the case of aluminum alloys, an oxidation reaction forms an oxide film layer on the surface of the metal, which acts as a protective coat by limiting weight loss over time [30, 31]. Furthermore, as the testing time increases, a continual effect of abrasives will be felt on the targeted surfaces. Due to the obvious continual impact, both uncoated AA6061 alloy and WC-10% Ni coating suffered from work hardening. The metal removal from the surface will be reduced as a result of this process [31]. When it comes to alloys, however, the work hardening effect is much stronger than when it comes to coatings.

#### 3.4. SEM Investigation of Slurry Eroded Surfaces.

Figure 11 shows slurry degraded surfaces of untreated and WC-10% Ni AA6061 alloy microstructures. When comparing untreated AA6061 alloy to WC-10% Ni specimens, it was discovered that the extent of the destruction is fairly severe. The coating thickness has minimized the damage to the surface, as seen in all microstructures. In general, metal removal in the course of a slurry erosion-corrosion experiment is connected with both erosion and corrosion mechanisms. Corrosion and erosion are the principal mechanisms of material loss in unprotected samples, as seen in SEM images by careful examination, which could be attributed to the aluminum alloy's weak corrosion and erosion wear resistance. When exposed to a slurry test, the corrosive medium has the ability to respond with the submerged surfaces of AA6061 alloy, forming a reactive interlayer. The continual mechanical action of slurry particles increases material removal in the slurry by removing the reactive layer, resulting in the exposure of fresh surface region as the corroded area, which offers inadequate protection to mechanical wear. The metal loss in the corroded zone is mostly due to its susceptible resilience to mechanical wear, as seen by the presence of corrosion pits in the micrographs [32].

In the subject of coatings, the experiment at a slurry content revealed that the degraded surface was encompassed by tiny cracks and raveling in multiple locations, as seen in Figure 11. Nonetheless, the level of spalling was low in the

context of WC-10% Ni coating, compared to that of uncoated AA6061 alloy. Despite the fact that the surfaces tested at greater slurry contents were contrasted, both surfaces showed significant spalling. In a recent situation, the degree of spalling is comparatively a lot less due to the rebounding of infringing particles and reciprocal collision, which reduces the efficacy to achieve the target. As the slurry content rises, so does the number of impinging particulates per unit volume. Because of mutual colliding and the bouncing effect, the velocity of impinging particulates decreases. Due to this, the targeted areas lose their route during the strike. As an outcome, the amount of particles attempting to reach the targeted area is modest when compared to those at a lower slurry content. This indicates why the weight reduction of the coating is significantly greater at greater slurry contents and significantly reduced at reduced slurry contents [33].

The eroded areas of unprotected AA6061 alloy and WC-10% Ni-coated AA6061 alloy are illustrated in Figures 12(a)–12(d) for slurry rotating speeds of 1500 rpm and 500 rpm. The eroded features of both the sample surfaces were created for the slurry rotating speed of 500 rpm using spallation, plastic deformations, and microcracks. The formation of spallation and microcracks is indicated by eroded micrographs as a key erosion mechanism.

The microcracks arise in coated samples as a result of continual abrasive particle impingement, and these microcracks begin to propagate in the directions of vulnerable areas, such as the interfaces or porosity between totally melted powdered particles and unmelted powdered particles. Whenever these microcracks cross, splats are removed at both the surface and subsurface levels. WC-10% Ni coatings have functionalities that relate to plastic deformations and a lot of microcracks. Due to the presence of WC-10% Ni, the surface experiences massive plastic deformation as a result of repetitive impacting of abrasives, resulting in a minimal weight reduction. In comparison to an unprotected AA6061 alloy, this is the fundamental reason why coating spalling is fairly low in the case of coatings due to abrasive's impact.

Nonetheless, with the increase of rotational speed to 1500 rpm, the degree of microcracks development and spalling increases significantly, especially for aluminum alloy. Because as the size and length of microcracks lengthen, spalling of large splats occurs [26, 33–35] and increasing rotating speed is expected to increase the erosion rate. The local stress rises of the susceptible interface between the completely molten and slightly melted splats and the increased rotational speeds, leading to microcracks in the WC-10% Ni protective covering. Figures 13(a)–13(d) shows the degraded surface of an alloy at 210  $\mu\text{m}$  particle size. The microcracks and shards of partially melted particles are visible in the WC-10% Ni coatings.

There were few craters of significant depth, indicating that coatings provide resilience. The presence of microcracks shows that the coatings have experienced substantial plastic straining as a result of the intersection between completely melted and unmelted particles, which has resulted in the production of microcracks. The susceptible intersection plays a crucial part as a maximum stress point because the strains tend to expand there, leading to the formation of



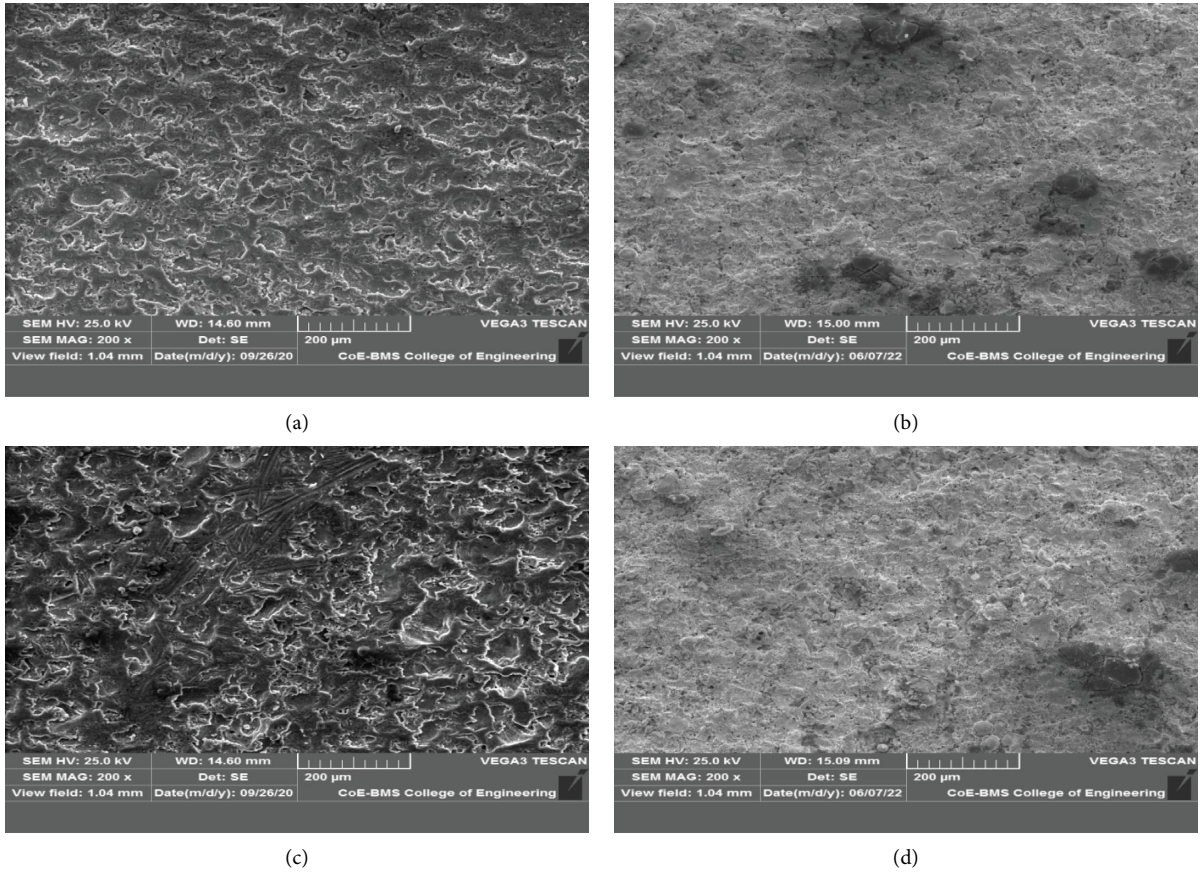


FIGURE 11: SEM of slurry eroded surfaces under different slurry concentrations: (a) Al6061 alloy (50 g/litre), (b) coatings (50 g/litre), (c) Al6061 alloy (200 gr/litre), and (d) coatings (200 gr/litre).

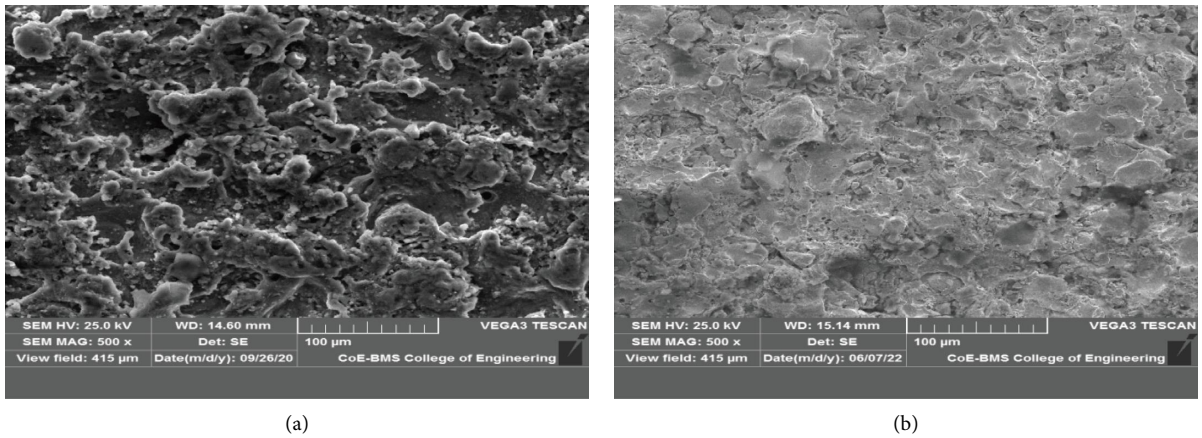
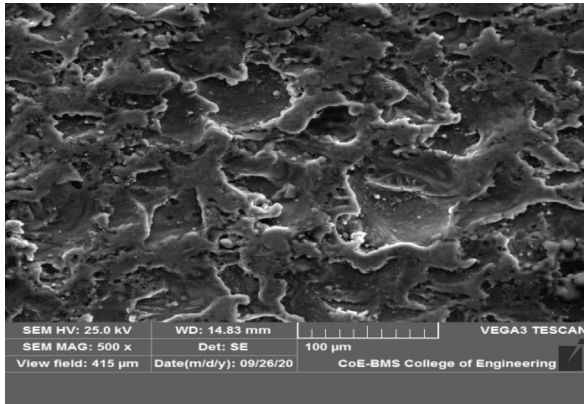
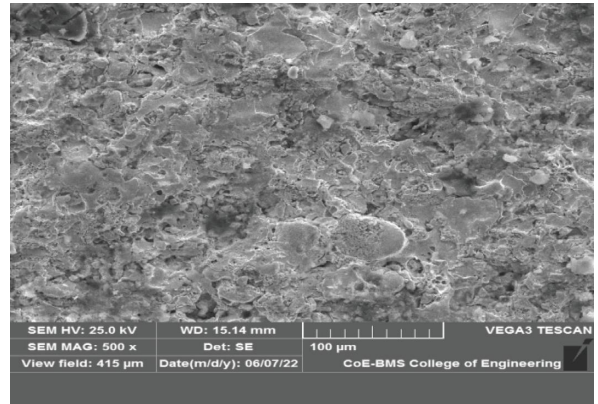


FIGURE 12: Continued.



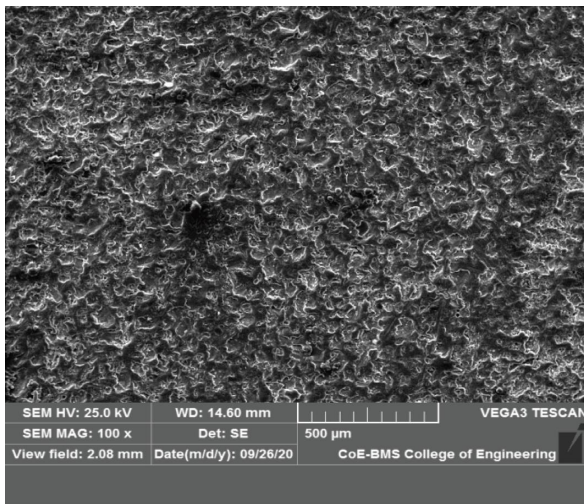


(c)

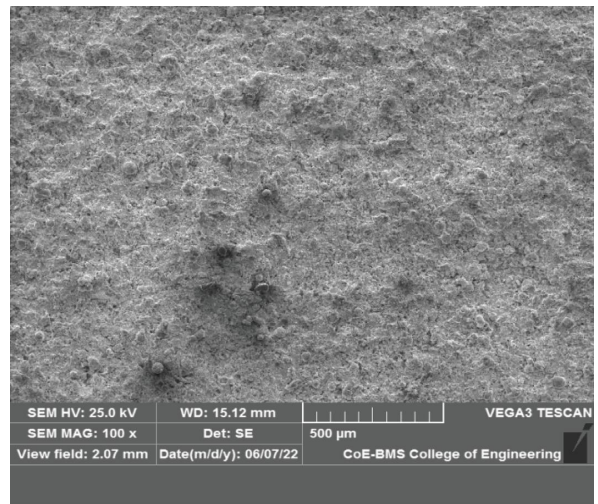


(d)

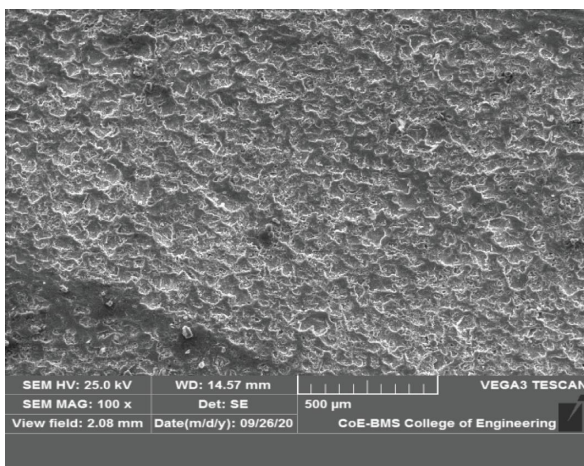
FIGURE 12: SEM of slurry eroded surfaces under different slurry speed: (a) Al6061 alloy (500 rpm), (b) coatings (500 rpm), (c) Al6061 alloy (1500 rpm), and (d) coatings (1500 rpm).



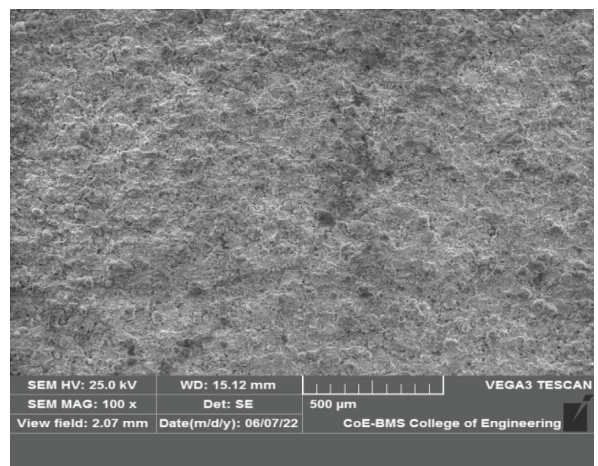
(a)



(b)



(c)



(d)

FIGURE 13: SEM of slurry eroded surfaces at different particle size: (a) Al6061 alloy (210 microns), (b) coatings (210 microns), (c) Al6061 alloy (625 microns), and (d) coatings (625 microns).

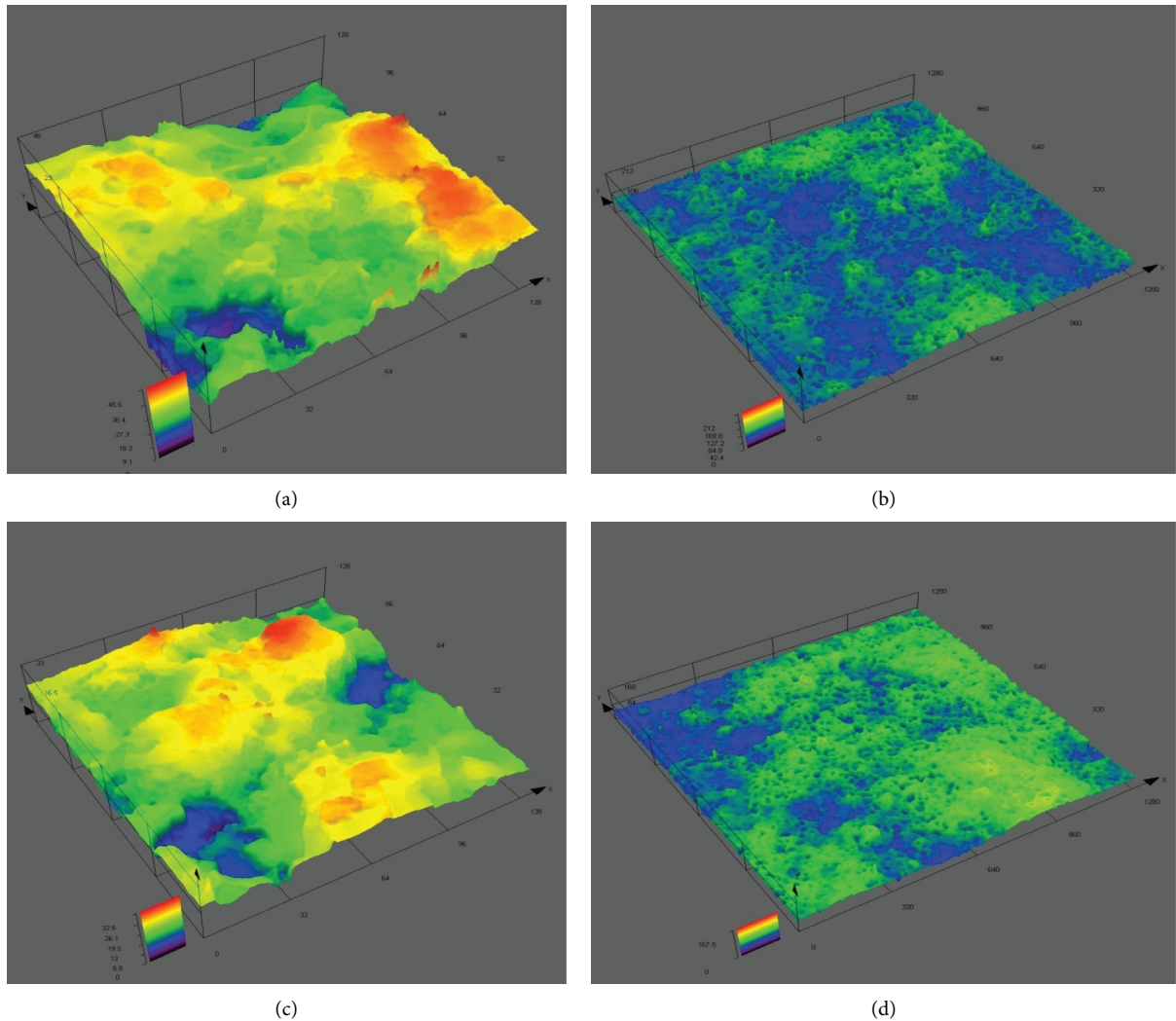


FIGURE 14: Confocal microstructures of slurry eroded surfaces at different slurry concentrations: (a) Al6061 alloy (50 g/litre), (b) Al6061-WC + Ni coating (50 g/litre), (c) Al6061 alloy (200 g/litre), and (d) Al6061-WC + Ni coating (200 g/litre).

microcracks. As demonstrated in the picture, the degraded surface regions of coated sample regions appear to be much softer at  $625\ \mu\text{m}$  particle size inspection compared to all those assessed at  $210\ \mu\text{m}$  particle size. The specimens are first subjected to erosion, however, as the particle increases, the lumps on the coated areas are removed. The knocking of protuberances occurs due to the repeated impact of abrasives, and the resulting stimulates the surface, which is softer at  $625\ \mu\text{m}$  particle size.

**3.5. Confocal Microscopy of Eroded Surfaces.** Figure 14 displays 3-D confocal microstructures of the slurry eroded areas of an unprotected AA6061 alloy and WC-10% Ni coatings tested at 120 N load. The highest width and height of the channels and holes are seen in unprotected AA6061 alloy, suggesting weak erosive resistance. On the other hand, high-velocity oxy-fuel-sprayed WC-10% Ni coatings have grooves and holes that are substantially smaller in width and height than the unprotected alloy. The surface area of aluminum alloys is much rougher and

sharper than those of WC-10% Ni coatings. These results corroborate the test results, indicating that WC-10% Ni coatings have a greater erosive resistance. Figures 14(a)–14(d) illustrates that the surface degradation of WC-10% Ni coatings is less than that of uncoated AA6061 alloy. These findings support the results of the slurry erosion examination, indicating that advanced WC-10% Ni coatings have enhanced resistance to slurry erosion. In case of unprotected AA6061 alloys, quite shallow contour patterns are observed; however, extensive surface grooves have been observed due to the particle effect. It is much more prevalent in unprotected eroded areas than in high-velocityoxy-fuel coatings, and this is supported by both experimentation and scanning electron microscope data. The residual depths of all high-velocityoxy-fuel coatings were observed to be much lesser than that of the unprotected AA6061 alloy (Figures 15(a)–15(d)) when tested at a slurry rotation of 500 rpm, 100 g/l slurry content, and  $625\ \text{m}$  impinging particle size for a testing period of five hours.



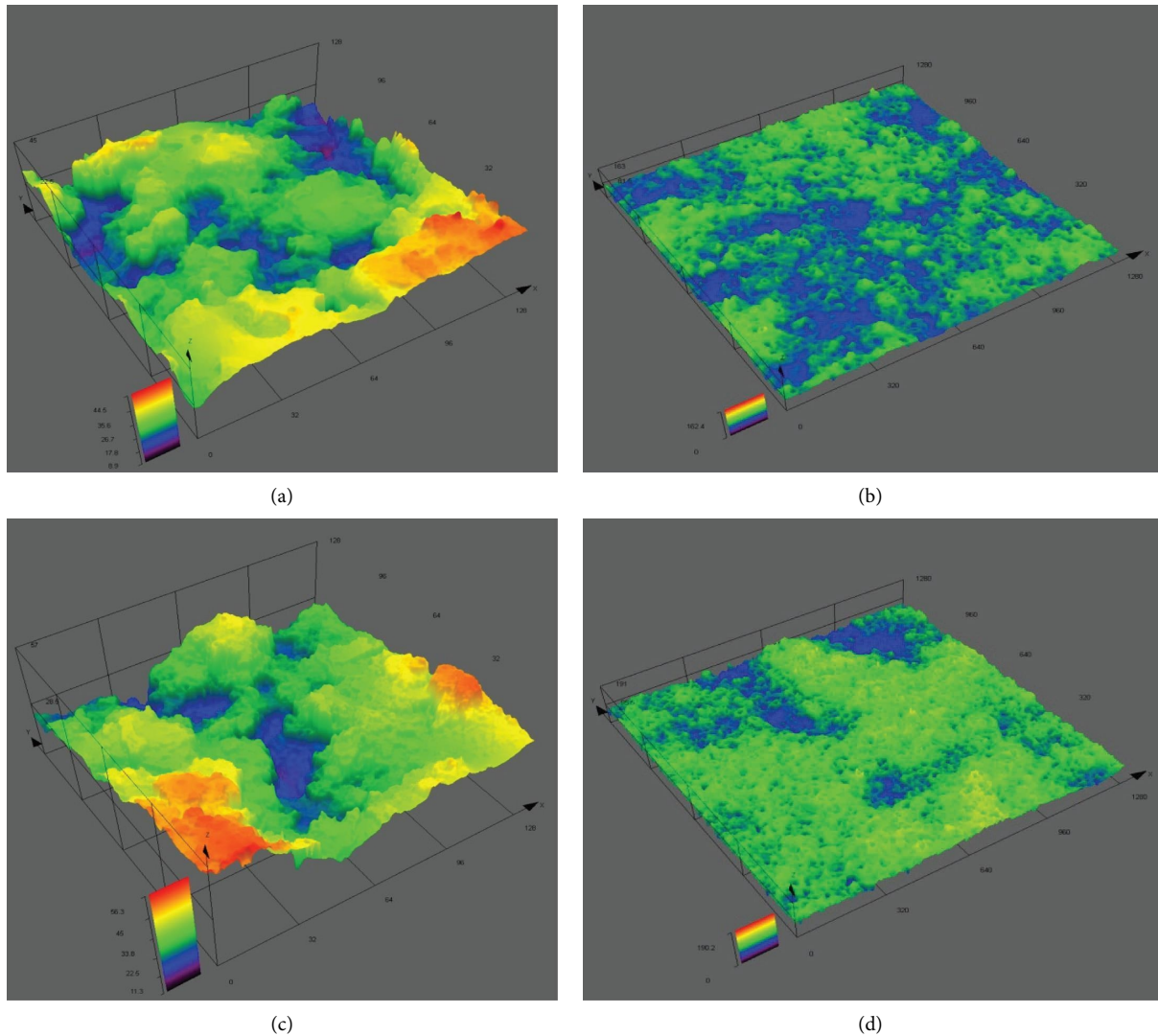


FIGURE 15: Confocal microstructures of slurry eroded surfaces at different particle sizes: (a) Al6061 alloy (210 microns), (b) Al6061-WC + Ni coating (210 microns), (c) Al6061 alloy (625 microns) and (d) Al6061-WC + Ni coating (625 microns).

The optimal range of erosion degradation for high-velocityoxy-fuel coatings was determined to be lesser than that for unprotected AA6061 aluminum alloy. In comparison to unprotected AA6061 alloy, high-velocity oxy-fuel-coated specimens with destroyed surface counts were found to be practically flat and it witnesses the homogeneous surface texture, as displayed in Figure 14. The degraded area contours of the unprotected AA6061 alloy specimens showed an inhomogeneous surface texture with uneven peaks in all of the conditions studied.

#### 4. Conclusions

High-velocity oxy-fuel-sprayed tungsten carbide with 10% nickel (WC-10% Ni) coatings of 100 m and 200 m thickness were successfully applied to an AA6061 aluminum alloy.

High-velocity oxy-fuel-sprayed WC-10% Ni coatings outperform AA6061 alloy in terms of slurry erosive resistance at all slurry speeds, particle sizes, and testing durations. The dense and homogeneous deposition of high-velocity oxy-fuel-sprayed WC-10% Ni coatings with increased hardness has improved slurry erosion-corrosion resistance. In terms of slurry wear resistance, high-velocityoxy-fuel sprayed WC-10% Ni coatings outperform untreated Al6061. Excessive weight losses in AA6061 alloy and WC-10% Ni coatings have been attributed to large particle sizes, faster slurry speeds, and high concentration. When it comes to particle size, the material removal rate begins to increase until the particle size approaches 400 m, at which point there is only a minor increase in weight loss. In all scenarios, coatings outperform the substrate. The experiment period was increased from 5 to 15 hours, resulting in greater

material removal on both the AA6061 substrate and the WC-10% Ni coatings. Following that, the weight loss appears to be very consistent. The results of this experiment revealed that WC-10% Ni coatings lasted longer under harsh conditions than in alloys. According to scanning electron microscope and confocal microscope examinations of worn-out surfaces, the wear was primarily caused by erosion, abrasion, corrosion, and collective and individual wear mechanisms.

## Data Availability

There are no data available apart from the data presented in this article. All data are available within the research article.

## Conflicts of Interest

The authors declare that they have no conflicts of interest.

## References

- [1] G. P. Kumar, R. Keshavamurthy, M. P. Akhil et al., "Friction and wear behavior of HVOF sprayed  $\text{Cr}_2\text{O}_3$ - $\text{TiO}_2$  coatings on aluminum alloy," *International Journal of Materials Engineering Innovation*, vol. 12, no. 1, pp. 1–7, 2021.
- [2] C. S. Ramesh, R. Keshavamurthy, and G. J. Naveen, "Effect of extrusion ratio on wear behaviour of hot extruded Al6061-SiCp(Ni- Pcoated) composites," *Wear*, vol. 271, pp. 1868–1877, 2011.
- [3] C. S. Ramesh and R. Keshavamurthy, "Slurry erosive wear behavior of Ni-P coated  $\text{Si}_3\text{N}_4$  reinforced Al6061 composites," *Materials and Design*, vol. 32, no. 4, pp. 1833–1843, 2011.
- [4] H. J. Amarendra, M. S. Prathap, S. Karthik et al., "Combined slurry and cavitation erosion resistance of HVOF thermal spray coated stainless steel," *Materials Today Proceedings*, vol. 4, no. 2, pp. 465–470, 2017.
- [5] J. F. Santa, L. A. Espitia, J. A. Blanco, S. A. Romo, and A. Toro, "Slurry and cavitation erosion resistance of thermal spray coatings," *Wear*, vol. 267, no. 1–4, pp. 160–167, 2009.
- [6] D. K. Goyal, H. Singh, H. Kumar, and V. Sahni, "Slurry erosive wear evaluation of HVOF-spray  $\text{Cr}_2\text{O}_3$  coating on some turbine steels," *Journal of Thermal Spray Technology*, vol. 21, no. 5, pp. 838–851, 2012.
- [7] D. W. Kim, S. I. Shin, J. D. Lee, and S. G. Oh, "Preparation of chromia nanoparticles by precipitation-gelation reaction," *Materials Letters*, vol. 58, no. 12–13, pp. 1894–1898, 2004.
- [8] B. S. Mann and B. Prakash, "High temperature friction and wear characteristics of various coating materials for steam valve spindle application," *Wear*, vol. 240, no. 1–2, pp. 223–230, 2000.
- [9] B. Guney and İ. Mutlu, "Wear and corrosion resistance of  $\text{Cr}_2\text{O}_3$ -40% $\text{TiO}_2$  coating on gray cast-iron by plasma spray technique," *Materials Research Express*, vol. 6, no. 9, Article ID 096577, 2019.
- [10] B. E. Naveena, R. Keshavamurthy, and N. Sekhar, "Comparative study on effects of slurry erosive parameters on plasma sprayed flyash- $\text{Al}_2\text{O}_3$  and flyash-SiC composite coatings on Al6061 alloy," *International Journal of Computational Materials Science and Surface Engineering*, vol. 8, no. 1, p. 57, 2019.
- [11] A. Koutsomichalis, M. Vardavoulis, and N. Vaxevanidis, "HVOF sprayed WC-CoCr coatings on aluminum: tensile and tribological properties," *IOP Conference Series: Materials Science and Engineering*, vol. 174, Article ID 012062, 2017.
- [12] B. E. Naveena, R. Keshavamurthy, and N. Sekhar, "Slurry erosive wear behaviour of plasma-sprayed flyash- $\text{Al}_2\text{O}_3$  coatings," *Surface Engineering*, vol. 33, no. 12, pp. 925–935, 2017.
- [13] C. S. Ramesh, N. Sekhar, R. Keshavamurthy, and S. Pramod, "A study on slurry erosion and corrosion behaviour of HVOF sprayed titania coatings," *International Journal of Surface Science and Engineering*, vol. 9, no. 1, pp. 55–68, 2015.
- [14] V. A. D. Souza and A. Neville, "Aspects of microstructure on the synergy and overall material loss of thermal spray coatings in erosion–corrosion environments," *Wear*, vol. 263, no. 1–6, pp. 339–346, 2007.
- [15] F. J. Hermanek, *Thermal spray Terminology and Company Origins*, ASM International, Materials Park, OH, USA, 2001.
- [16] P. Vuoristo, *Thermal spray Coating Processes, Comprehensive Materials Processing Volume: Coatings and Films*, Elsevier, Amsterdam, Netherlands, 2014.
- [17] R. J. Talib, S. Saad, M. R. M. Toff, and H. Hashim, "Thermal spray coating technology—a review," *Solid State Sci Technol*, vol. 11, no. 1, pp. 109–117, 2003.
- [18] M. L. Thorpe, "Thermal spray: industry in transition," *Advanced Materials and Processes*, vol. 143, no. 5, pp. 50–56, 1993.
- [19] M. I. Boulos, *Thermal spray Fundamentals, from Powder to Part*, Springer Science+Business Media, New York, NY, USA, 2014.
- [20] R. Keshavamurthy, B. E. Naveena, and N. Sekhar, "Thermal spray coatings for erosion-corrosion protection," in *Production, Properties, and Applications of High Temperature Coatings*, pp. 246–267, IGI Global, Hershey, PA, USA, 2018.
- [21] K. Farokhzadeh, R. M. Fillion, and A. Edrissy, "The effect of deposition rate on microstructural evolution in WC-Co-Cr coatings deposited by high-velocityoxy-fuel thermal spray process," *Journal of Materials Engineering and Performance*, vol. 28, no. 12, pp. 7419–7430, 2019.
- [22] G. S. P. Kumar, A. Shinde, Y. Yadav, G. S. Hebbar, and M. H. Kumar, "Investigations on slurry erosive on wear performance of HVOF-sprayed  $\text{Cr}_2\text{O}_3$  coatings on aluminum alloy," *Journal of Bio- and Tribo-Corrosion*, vol. 7, no. 3, p. 106, 2021.
- [23] S. H. Mousavi Anijdan, A. Bahrami, N. Varahram, and P. Davami, "Effects of tungsten on erosion–corrosion behavior of high chromium white cast iron," *Materials Science and Engineering A*, vol. 454–455, pp. 623–628, 2007.
- [24] K. Bandil, H. Vashisth, S. Kumar et al., "Microstructural, mechanical and corrosion behaviour of Al-Si alloy reinforced with SiC metal matrix composite," *Journal of Composite Materials*, vol. 53, no. 28–30, pp. 4215–4223, 2019.
- [25] P. Vijay1, K. V. Brahma Raju, K. Ramji, and S. Kamaluddin, "Effect of tungsten carbide on al6061/sic hybrid metal matrix composites," *Composites theory and practice*, vol. 21, no. 4, pp. 169–180, 2021.
- [26] H. S. Grewal, H. S. Arora, A. Agrawal, H. Singh, and S. Mukherjee, "Slurry erosion of thermal spray coatings: effect of Sand concentration," *Procedia Engineering*, vol. 68, pp. 484–490, 2013.
- [27] A. Mansouri, M. Mahdavi, S. A. Shirazi, and B. S. McLaury, "Investigating effect of sand concentration on erosion rate in slurry flows," in *Proceedings of the International Corrosion Conference*, Montpellier, France, September 2005.

- [28] K. Anand, S. K. Hovis, H. Conrad, and R. Scattergood, "Flux effects in solid particle erosion," *Wear*, vol. 118, no. 2, pp. 243–257, 1987.
- [29] R. S. Lynn, K. K. Wong, and H. M. Clark, "On the particle size effect in slurry erosion," *Wear*, vol. 149, no. 1-2, pp. 55–71, 1991.
- [30] S. Turenne, D. Simard, and M. Fiset, "Influence of structural parameters on the slurry erosion resistance of squeeze-cast metal matrix composites," *Wear*, vol. 149, no. 1-2, pp. 187–197, 1991.
- [31] S. Turenne, Y. Chatigny, D. Simard, S. Caron, and J. Masounave, "The effect of abrasive particle size on the slurry erosion resistance of particulate-reinforced aluminium alloy," *Wear*, vol. 141, no. 1, pp. 147–158, 1990.
- [32] C. S. Ramesh, R. Keshavamurthy, B. H. Channabasappa, and S. Pramod, "Influence of heat treatment on slurry erosive wear resistance of Al6061 alloy," *Materials and Design*, vol. 30, no. 9, pp. 3713–3722, 2009.
- [33] R. Keshavamurthy, B. E. Naveena, A. Ahamed, N. Sekhar, and D. Peer, "Corrosion characteristics of plasma sprayed flyash–SiC and flyash–Al<sub>2</sub>O<sub>3</sub> composite coatings on the Al-6061 alloy," *Materials Research Express*, vol. 6, no. 8, Article ID 08654, 2019.
- [34] V. L. Ratia, D. Zhang, J. L. Daure, P. H. Shipway, D. G. McCartney, and D. A. Stewart, "Sliding wear of a self-mated thermally sprayed Chromium oxide coating in a simulated PWR water environment," *Wear*, vol. 426-427, pp. 1466–1473, 2019.
- [35] T. Ohmi, Y. Nakagawa, M. Nakamura, A. Ohki, and T. Koyama, "Formation of chromium oxide on 316L austenitic stainless steel," *Journal of Vacuum Science and Technology*, vol. 14, no. 4, pp. 2505–2510, 1996.